Research Article | Vol. 31, No. 22 / 23 Oct 2023 / Optics Express 36928
Optics EXPRESS

Non-destructive characterization of nested and double nested antiresonant nodeless fiber microstructure geometry

LEONARD BUDD,* ERIC NUMKAM FOKOUA, AUSTIN TARANTA, AND FRANCESCO POLETTI

Optoelectronics Research Centre, University of Southampton, SO17 1BJ, UK
*l.g.budd@soton.ac.uk

Abstract: Antiresonant hollow-core fibers (HCFs) are rapidly establishing themselves as a promising technology with the potential to overcome the limitations faced by conventional solid-core silica fibers. The optical properties and performance of these fibers depend critically on the precise control and uniformity of their delicate glass microstructure at all points along the length of the fiber. Their fabrication is complicated by the inability to monitor this microstructure without cutting into the fiber and viewing a sample under a microscope during the fiber draw. Here we show that a non-destructive interferometric technique using side-illumination of the fiber and first demonstrated for simple tubular fibers can be used to measure the diameters of all nested capillary elements of two promising HCF designs: the nested and double-nested antiresonant nodeless fiber (NANF and DNANF, respectively) with accuracy comparable to a microscope measurement. We analyze the complexities enabled by the presence of multiple nested capillaries in the structure and present techniques to overcome them. These measurements, carried out on a small (~50 cm) length of fiber, require less than 60s to collect and process the data for all capillaries. We also show how we can use this technique to detect defects in the fiber, making it a potential candidate for real-time in-situ monitoring of NANF and DNANF structures during fabrication.

1. Introduction

Since the advent of hollow-core photonic bandgap fibers (HC-PBGFs) in the late 1990s, researchers have demonstrated many advantages of optical fibres which confine light in hollow core rather than a solid glass one [1]. Light propagating in air experiences orders of magnitude lower Rayleigh scattering and optical non-linearity than bulk silica, offering the attractive prospect of overcoming the limits of conventional silica fiber technology in many key application areas. Interest in hollow core optical fibers has been renewed by the development of antiresonant fibers in the early 2010s [2]. These fibers guide light at antiresonant wavelengths governed by the geometry of a surrounding glass microstructure. Guiding light in this way can offer a wider bandwidth than in PBGFs and the minimization of the electric field at the air-glass interface can help reduce the loss incurred from surface roughness scattering. Of particular interest are nested antiresonant and double nested antiresonant nodeless fibers (NANFs [3] and DNANFs [4] respectively). The microstructure of these fibers consists of multiple sets of nested glass capillaries surrounding the central core. In NANF and DNANF, each set consists of two and three nested elements respectively. Since the first proposal of these fiber designs in 2014, the process of fabricating these fibers has improved to the extent that the loss has reduced from around 100 dB/km in the first feasibility demonstrations [5,6], to 0.174 dB/km in the C-band in 2022 [4] - currently the lowest loss reported for any hollow core fiber and on par with commercial

#504992 https://doi.org/10.1364/OE.504992
Journal © 2023 Received 7 Sep 2023; revised 9 Oct 2023; accepted 10 Oct 2023; published 17 Oct 2023

Optics EXPRESS

single mode fibers. Meanwhile, hollow core fibers can now offer fundamentally lower loss than solid silica fibers across the visible and mid infrared spectral regions. In addition to low loss, these fibers also present backscattering over 40 dB lower than silica fibers [7] and polarization mode cross-coupling around three orders of magnitude lower than state-of-the-art polarization maintaining solid core fibers [8].

The optical performance of these fibers is highly governed by the geometry of their inner microstructure. The wavelengths at which the fiber will guide light are determined by the thickness of the glass membranes that surround the core. The effectively single-moded operation of certain NANF and DNANF designs relies on correctly sizing the cavities delimited by the nested capillaries, such that higher order modes propagating in the core are strongly coupled to those therein and are 'stripped' away [9] during propagation. Additionally, the loss of these fibers is highly sensitive to the gaps between neighboring capillaries. If these capillaries come into contact with each other, 'nodes' are formed. These nodes form local waveguides, supporting glass-propagating modes that can couple with the fundamental core mode and greatly increase the loss of the fiber. It is therefore vital to have some method for monitoring microstructure geometry during fiber fabrication to ensure that the required geometry is being reached and maintained during the fiber draw. This is currently achieved by collecting and analyzing fiber samples under a microscope during the draw and then making any necessary adjustments to the various draw control parameters. There are numerous disadvantages to this process: the fiber is cut, decreasing the overall yield of the draw. The process is slow; while the analysis of the sample is taking place many meters of sub-optimal fiber may still be being fabricated. Defects may also occur between sample points, meaning that they are not discovered until the optical performance of the fiber is characterized, for example through loss measurements or OTDR. A method of rapidly and non-destructively characterizing the microstructure geometry during fabrication is therefore highly desirable.

While solutions for non-destructive structural monitoring have long been readily available for standard silica fiber [10,11], allowing full automation of the fabrication process and facilitating their mass production, the presence of the glass microstructure and air core significantly complicates the problem for hollow core fibers. Previously reported non-destructive measurement techniques have included using X-ray tomography to characterize PBGFs and their preforms [12]. Whilst providing high spatial accuracy and a full 3D reconstruction of the fiber geometry, the timescales involved with each scan (30 minutes to 12 hours) make this technique unsuitable for inline monitoring. Another tomographic method relying on the Doppler-shifted scattered light from a continuously rotating fiber showed the potential to reconstruct the cross-section of a solid core photonic crystal fiber [13]. However, the need to spin either the fiber or detector makes this technique challenging to implicate in all fabrication environments. A side-scattering method for accurately determining the diameter of the central air core of a capillary fiber was demonstrated in 2017 [14]. Whilst rapid and non-destructive, such a technique is not easily applicable to the complex microstructure of NANFs and DNANFs.

Here we report non-destructive measurements of NANF and DNANF microstructure geometry utilizing a side scattering interferometric technique first experimentally demonstrated for both offline and real-time measurements of tubular fibers (ARFs with no nested capillary elements) and modeled for fibers with a single nested element [15]. We expand on the results first presented in [16,17] and show that this technique can be used to non-destructively measure the diameters of all nested capillaries, as well as detect contact points between neighboring capillaries. This technique is rapid (<0.1s to collect and analyze a measurement) and optically safe due to the low power of the source, making it potentially suitable for real-time monitoring of the microstructure during fabrication.

Optics EXPRESS

2. Method

A schematic of the experimental setup is shown in Fig. 1(a). Light from a broadband light source *WLS* is coupled into multi-mode fiber *MM1* and then collimated by lens *L* onto the side of the hollow core fiber under test *HCF*. An example source spectrum is shown in Fig. 1(b). *HCF* is vertically mounted between two motorized rotation stages, allowing full rotation of the fiber and all capillaries to be probed. A polarizing beam splitter *PBS* ensures that only one polarization of modes are excited around the fiber capillaries. A portion of the light scattered from the *HCF* is collected by multi-mode fiber *MM2* and fed into a spectrometer connected to a computer. The collection angle θ between the incoming light and the end facet of the collection fiber is an important parameter to optimize in order to provide an unambiguous measurement of the microstructure [15,18]. We require maximum interferometric contrast between light entering the microstructure and light traversing just the surrounding jacket tube, whilst also wanting to minimize the spurious 'difference' signals first experimentally demonstrated in [16,17].

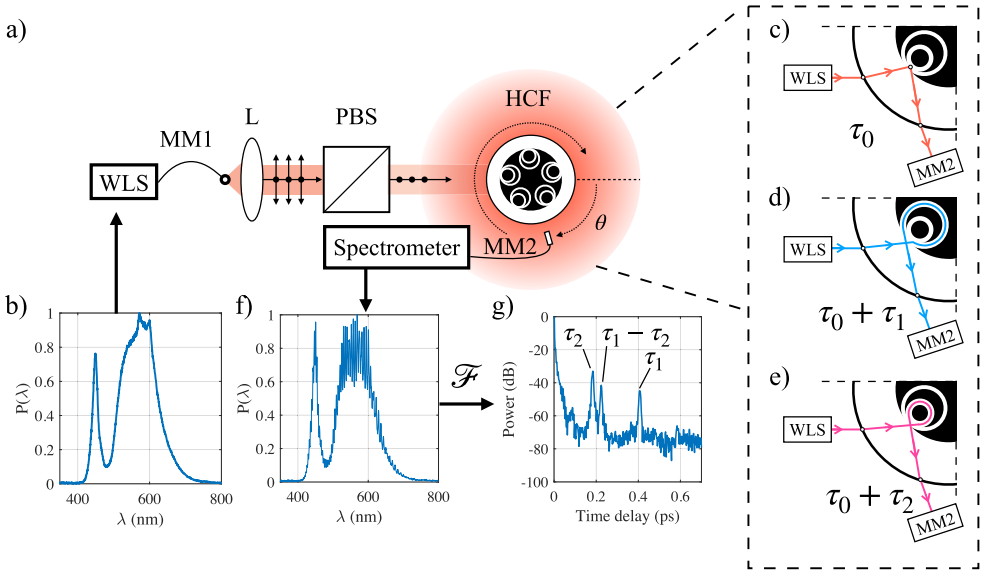

Fig. 1. (a) Diagram of experimental setup (b) Spectrum of LED source. (c-e) Optical paths inside fiber *HCF*. (f) Typical side-scattering spectrum showing interference pattern. (g) IFT of scattering spectrum with time delay peaks corresponding to interference between the optical paths shown in (c-e).

Upon entering the fiber, some of the light is reflected off the air-glass interface between the central hollow core and surrounding glass jacket tube (Fig. 1(c)), taking some time τ_0 before reaching the collection fiber *MM2*. For NANF, fractions of this light couple into the outer and inner capillaries of the fiber (Fig. 1(d) and (e) respectively), taking additional amounts of time τ_1 and τ_2 to arrive at *MM2*. Constructive and destructive interference between light traversing these various optical paths manifests itself as an oscillating interference pattern in the spectral domain as shown in Fig. 1 f. An inverse Fourier transform (IFT) of this spectrum (Fig. 1 (g)) shows time delay peaks corresponding to τ_1 and τ_2, as well as an extra 'difference' signal located at $\tau_1 - \tau_2$. The origin of this difference signal can be understood by considering the various interfering fields that exit the fiber. We write the electric field of the 'reference' ray with time delay τ_0 as $E_0 \exp(-i\phi)$ for some arbitrary amplitude E_0 and phase ϕ. The rays that enter the outer and inner capillaries with diameters d_1 and d_2 respectively can be written as $\eta_1 E_0 \exp(-i(\phi + \beta\pi d_1))$ and $\eta_2 E_0 \exp(-i(\phi + \beta\pi d_2))$. Here $\eta_{1,2}$ are coupling coefficients representing the fractions of light

Optics EXPRESS

that traverse the inner and outer capillaries respectively. We treat the fiber capillary as a planar waveguide of equivalent thickness and associated propagation constant β. This approximation is valid providing the diameter is much larger than the thickness of the capillary [19]. For illustrative purposes, we assume that the round trip of the capillary is the only factor that leads to a phase difference between the various electric fields. The total, time-averaged optical power in the spectral domain $P(\omega)$ incident on the detector can therefore be written as

$$P(\omega) = \left| E_0(\omega) e^{-i\phi} + \eta_1 E_0(\omega) e^{-i(\beta\pi d_1+\phi)} + \eta_2 E_0(\omega) e^{-i(\beta\pi d_2+\phi)} \right|^2. \tag{1}$$

Applying an IFT to the time domain yields

$$P(t) = \mathcal{F}(|E_0|^2) * \left[A(t) \left(1 + \eta_1^2 + \eta_2^2\right) + \eta_1 A(t-\tau_1) + \eta_2 A(t-\tau_2) + \eta_1\eta_2 A(t-(\tau_1-\tau_2)) \right], \tag{2}$$

Where $A(t')$ is the coherence function of the light source which peaks at $t' = 0$. We therefore expect three peaks, with the two at $t = \tau_1$ and $t = \tau_2$ corresponding to the time delay accrued around the outer and inner capillaries, and an additional difference signal at $t = \tau_1 - \tau_2$. It should be noted that, due to taking the complex conjugate of the electric field in Eq. (1), the 'sum' signal at $t = \tau_1 + \tau_2$ predicted by modeling in [15] does not appear experimentally. Repeating this analysis for DNANF with an additional nested element ($d_1 > d_2 > d_3$) gives

$$\begin{aligned} P(t) = \mathcal{F}(|E_0|^2) * \Big[& A(t)\left(1 + \eta_1^2 + \eta_2^2 + \eta_3^2\right) + \eta_1 A(t-\tau_1) + \eta_2 A(t-\tau_2) + \eta_3 A(t-\tau_3) + \cdots \\ & \eta_1\eta_2 A(t-(\tau_1-\tau_2)) + \eta_1\eta_3 A(t-(\tau_1-\tau_3)) + \eta_2\eta_3 A(t-(\tau_2-\tau_3)) \Big]. \end{aligned} \tag{3}$$

Again we see the peaks for each capillary at τ_1, τ_2 and τ_3. There are now however three difference signals, one for each of the pairwise combinations of τ_1, τ_2 and τ_3. This analysis which assumes that the interfering fields have the same spatial distribution and perfect spatial overlap suggests that, being proportional to the product of the coupling coefficients, the amplitude of difference signals in NANF and DNANF will be orders of magnitude smaller than the signals from the capillaries themselves. In practice, however, the difference signals can have comparable or even greater amplitude than the capillary signals. We can illustrate this by considering the spatial distributions of the electric fields arriving at the detector. In the case of NANF, the optical power in the spectral domain can be written as

$$P(\omega) = \iint \left| E_0(x,y,\omega) e^{-i\phi} + E_1(x,y,\omega) e^{-i(\beta\pi d_1+\phi)} + E_2(x,y,\omega) e^{-i(\beta\pi d_2+\phi)} \right|^2 dx\, dy, \tag{4}$$

where $E_{0,1,2}$ now have both a spatial and spectral dependence. For illustrative purposes, we take these profiles to be Gaussian for all three electric fields. We can express $E_{0,1,2}$ as:

$$E_0(x,y,\omega) = e^{-\frac{x^2+y^2}{2w_0^2} - \frac{(\omega-\omega_0)^2}{2\Delta\omega^2}}, \tag{5}$$

$$E_1(x,y,\omega) = \eta_1 e^{-\frac{(x-x_1)^2+(y-y_1)^2}{2w_1^2} - \frac{(\omega-\omega_0)^2}{2\Delta\omega^2}}, \tag{6}$$

$$E_2(x,y,\omega) = \eta_2 e^{-\frac{(x-x_2)^2+(y-y_2)^2}{2w_2^2} - \frac{(\omega-\omega_0)^2}{2\Delta\omega^2}}. \tag{7}$$

Here, E_0 is centered at $(0,0)$ with waist w_0, $E_{1,2}$ is centered at $(x_{1,2}, y_{1,2})$ with waist $w_{1,2}$. ω_0 is the central frequency of the beams and $\Delta\omega$ is the spectral width. As before, we can apply an IFT to Eq. (4) and calculate the amplitude of the difference signals for a range of spatial separations and coupling coefficients.

Optics EXPRESS

Figure 2(a) shows the variation in difference signal from a NANF for three different separations between the beams from the inner and outer capillaries. When the beams are far apart relative to their waists, no difference signal is present. Bringing the beams closer together increases the power of the difference signal, to the extent that when their separation is comparable to the beam waist, the difference signal is more powerful than the inner and outer capillary signals, despite the product of the small coupling coefficients. Similarly, Fig. 2(b) shows the effect of varying this coupling coefficient on the relative power of the difference signal. Even for a coupling coefficient as low as 0.001, if the separation between the two beams is sufficiently small, the difference signal can still be at a comparable power to the inner and outer capillary signals. This can lead to difficulty determining which peak corresponds to an actual capillary diameter and which is a difference signal, particularly problematic when trying to measure the innermost capillaries of NANF and DNANF. As discussed further below, we can overcome this issue by adjusting the collection angle (θ in Fig. 1(a)) such that the spatial overlap between the capillary beams is minimized.

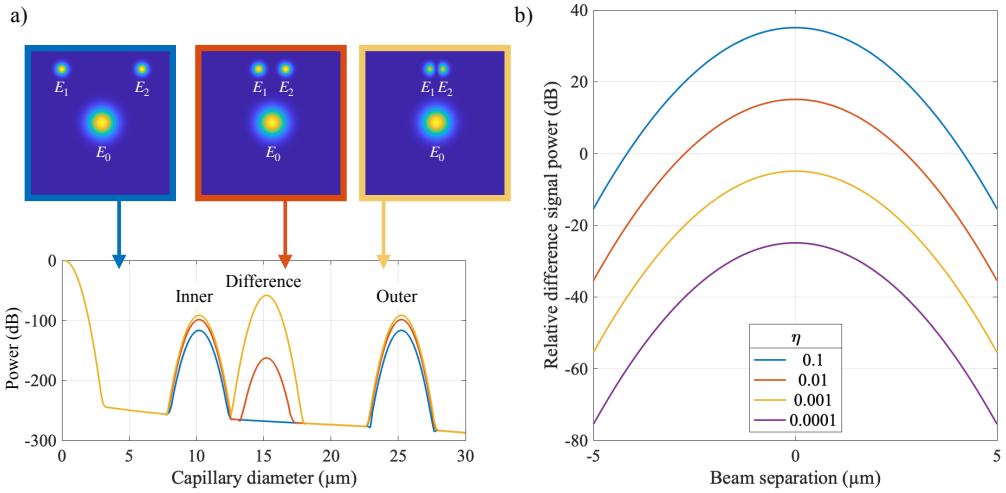

Fig. 2. Calculated difference signals from a NANF with a 25μm outer capillary and a 10μm inner capillary. E_0 has a waist of 2μm and $E_{1,2}$ both have a 1μm waist. The central wavelength is 600nm for all beams. We assume that the coupling coefficient into the inner and outer capillaries is the same ($\eta_1 = \eta_2 = \eta$). (a) Example traces for separations of 10μm (blue), 5μm (orange) and 2.5μm (yellow) between E_1 and E_2. Here, $\eta = 0.1$. The colormaps show $P(x, y)$ at 600 nm for all three separations. (b) Difference signal power relative to inner and outer signals as function of separation between E_1 and E_2 for a range of different coupling coefficients η.

2.1. *Extracting capillary diameter*

Having shown the existence of time domain peaks dependent on the geometry of NANF and DNANF microstructure, it is necessary to convert these time delays to an equivalent capillary diameter. The expected time delay for a given fiber geometry can be calculated using the geometrical optics model described in [18] for tubular fibers. This model can straightforwardly be applied to NANF and DNANF by adding additional capillaries. Whilst precise calculation of the time delay peak requires knowing every dimension of the microstructure geometry, we can still obtain an accurate measurement of capillary diameter with limited information about the fiber. To illustrate this, we use a sensitivity analysis to the geometrical formulae presented in [18] to determine which microstructure aspects contribute most to the position of the time delay

Optics EXPRESS

peak. The dimensions affecting the optical path delay are shown in Fig. 3 a and b. These are the outer and inner radii of the jacket tube (R and r respectively), capillary diameter d, capillary thickness t and capillary inset into the jacket tube δ. This inset arises from fusing the capillary to the jacket tube during fabrication of the preform. Considering a typical fiber geometry (R=100 µm, r=40 µm, d=14 µm and δ=1 µm), we vary each parameter in turn and calculate the resulting change in optical delay between the two paths using the analysis presented in [18]. Increasing R and r by 10% leads to path delay changes of 0.16 and 0.14% respectively - a negligible impact on the position of the time delay peak. Similarly, increasing δ by 10% causes the optical path delay to decrease by 0.3%. To consider the effect of the capillary thickness on the optical time delay, we calculate the group index of the fundamental TE mode for thicknesses between 400-600 nm (Fig. 3(c)). This range encompasses most typical target membrane thicknesses for both NANF and DNANF. In the range the light source operates (400-750 nm), the group index varies by approximately 2%. Conversely, increasing the capillary diameter by 10% causes a 10.3% increase in the optical path delay. The larger than expected path delay increase can be attributed to the capillary ray's increased path length in the jacket tube. Capillary diameter is by far the most significant driver of time delay peak positions, and can be accurately measured (to within <2%) by applying a simple linear scaling to the time domain.

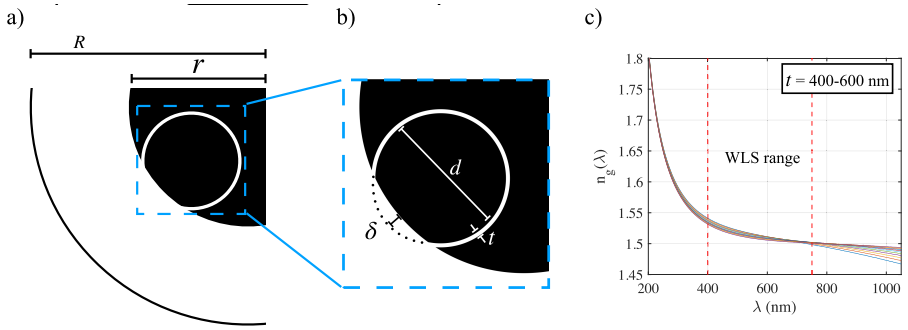

Fig. 3. (a) HCF jacket tube geometry. (b) HCF capillary geometry. (c) Group index of fundamental TE mode for planar waveguide thicknesses between 400-600 nm.

Another finding of [15] is that as the tubular fiber is rotated, the position of the time delay peaks vary, following a parabolic shape determined by the dimensions of the fiber. To show that this applies to NANFs as well, Fig. 4 shows example results from a full rotation of a NANF. Here we used a Thorlabs MWWHF2 WLS coupled into a 400 µm core diameter fiber. The output of this large mode area multimode fiber was collimated onto the side of an HCF. The NANF under test was rotated by two Zaber XRSW60-A motorized rotation stages and spectra were taken across a full HCF rotation with an angular resolution of 1°. Scattered light was captured by a 600 µm core diameter fiber coupled into an Ocean Insight FLAME spectrometer. An integration time of 60 ms was found to be suitable for these measurements. A full rotation of the fiber, collecting spectra every degree, therefore takes around 30s. We see the same parabolic effect for both NANF and DNANF, best illustrated by combining all 360 time traces for a complete HCF rotation and plotting them as a surface of power vs fiber rotation and time delay (Fig. 4(a) and (b)). On this surface, there are clear 'hotspots' separated by ~72 °, for each of the 5 HCF capillaries sets. The spaces between these hotspots are locations when the incoming beam is incident on gaps between neighboring capillaries and no interference signal is detected. The time delay position τ at the vertex of each parabola corresponds to the shortest optical path of the capillary ray where the extra optical path delay accrued in the jacket tube is minimized. We can therefore obtain an accurate measurement of capillary diameter d_c by applying the linear scaling

Optics EXPRESS

from [15]:

$$d_c \approx \frac{c}{\pi n_g}\tau, \tag{8}$$

for some planar waveguide group index n_g. To determine the parabola vertex, we can consider the variation in the maximum time domain power for a particular time domain bin. For example, in Fig. 4(c) we consider the 0.35-0.45 ps region, corresponding to the outer capillary of a NANF. Here there are five distinct peaks, the positions of which we use to determine the time traces that will provide the best measurement of capillary diameter.

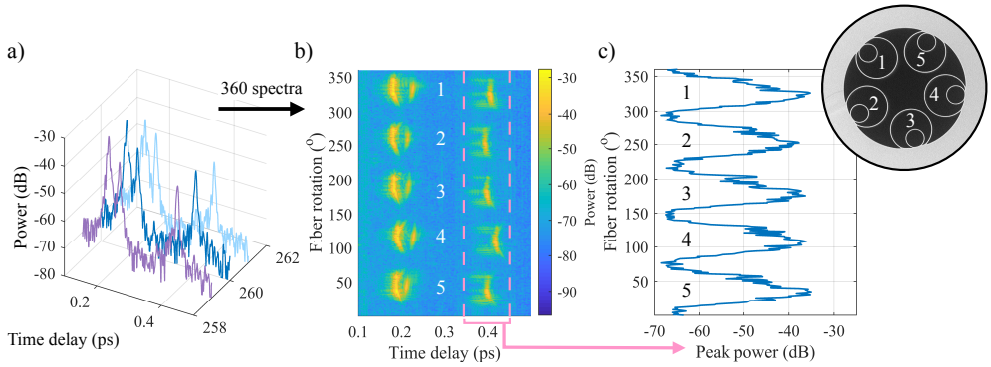

Fig. 4. (a) Example time delay traces captured at 3 different NANF rotation angles. (b) 360 time delay traces taken across a full HCF rotation plotted as a surface of time domain power vs time delay and fiber rotation. (c) Peak power in the 0.35-0.45 ps time bin.

3. Results

The results presented here use the same experimental setup shown and described in Section 2. We present non-destructive measurements of three different fibers: a NANF and DNANF both with good microstructure, and a NANF where two adjacent outer capillary elements are contacting.

3.1. NANF

Figure 5(a) shows an scanning electron microscope (SEM) image of the cross-section of the NANF used for this experiment. It has a microstructure comprised of 5 sets of nested capillaries, with microscope measurements indicating a mean outer capillary diameter d_1 of 26.6 µm and a mean inner capillary diameter d_2 of 12.1 µm. An IFT of a single side-scattering spectrum is shown in Fig. 5(b), with the time delay axis scaled to capillary diameter using the method detailed above. This trace corresponds to a measurement of capillary 3 in Fig. 5(a). As mathematically predicted, three peaks are visible on this trace: the outer capillary d_1 at 25.8 µm, inner d_1 at 11.8 µm and the difference signal ($d_{12} = d_1 - d_2$) at 14.0 µm as expected. The peak power in the inner and outer capillary regions is plotted in Fig. 5(c). There is a mean offset of 10° between the maxima of the inner and outer signals, confirming that the centers of the two nested elements are not at the same angular position on the outer jacket wall. Applying the linear scaling method at the inner and outer maxima locations yields non-destructive measurements of all 5 nested capillaries, plotted in Fig. 5(d) and compared with SEM measurements. The average discrepancy between the microscope and non-destructive measurements is 140 nm (1.2%) for the inner capillaries and 180 (0.7%) for the outer capillaries.

The results in Fig. 5 were taken at a collection angle of 60°. This value was chosen to in order maximize the SNR of the inner and outer capillary signals, whilst minimizing the power of the difference peak. This value was chosen empirically based on the collection angle investigation

Optics EXPRESS

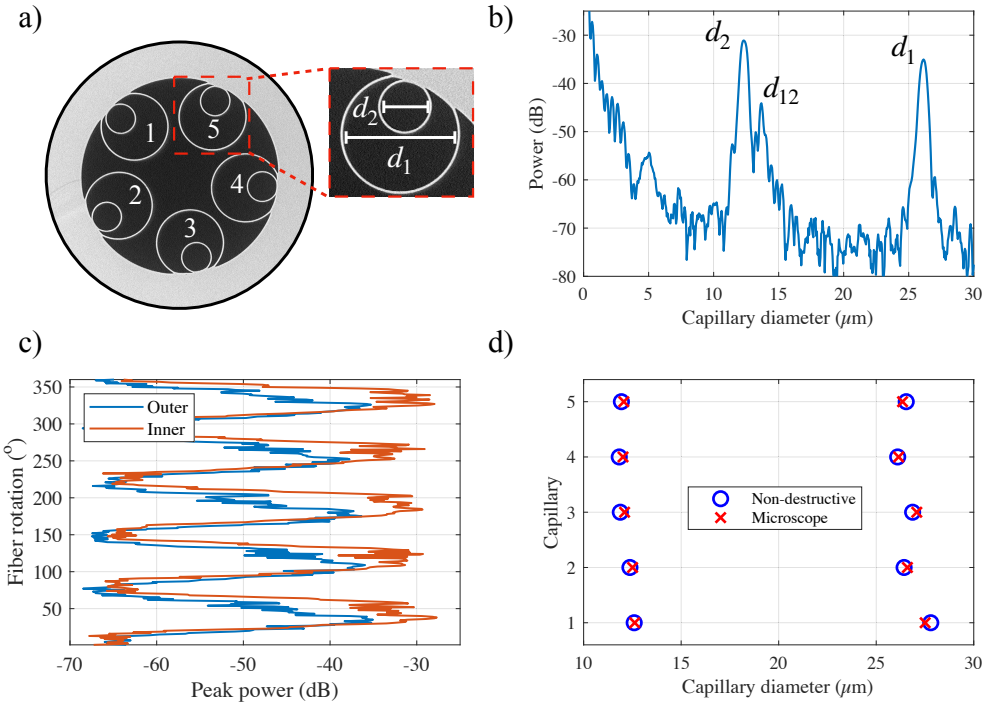

Fig. 5. NANF results. (a) SEM image of NANF cross-section. (b) Capillary diameter plot showing peaks corresponding to inner, outer and difference signals. (c) Peak power of inner and outer capillaries across a full fiber rotation. (d) Non-destructive and microscope measurements of inner and outer capillary diameters.

shown in Fig. 6. Here, side scattering spectra were taken for a complete rotation of the NANF in Fig. 5(a) for a range of collection angles from −100°. to +100°. Positive and negative collection angles correspond to values of θ below and above the dotted line in Fig. 1(a) respectively. Figure 6(a) shows the SNR of the inner and outer capillary peaks as a function of collection angle. This peaks at ±70° for the outer capillary, and ±90° for the inner. For collection angles less than ±40°, the contrast between the incoming light from the source and the light interacting with the microstructure is too low to provide a reliable measurement of the NANF capillaries. ±90° is an unsuitable choice for the collection angle as the difference signal is very prominent, as illustrated in Fig. 6(b). Here, we calculate the difference signal power by considering the positions of the two beams leaving the inner and outer capillaries relative to the reference beam. This is done using the expressions for the angles of the beams exiting the fiber presented in [18]. Using these separations with Eq. (4) yields a difference signal power which agrees well with experimental results. From this, we can see that decreasing the collection angle also decreases the prominence of the difference signal relative to the inner and outer capillaries. A choice of ±60° therefore ensures a good SNR for both inner and outer capillaries, whilst minimizing the difference signal. This allows us to unambiguously determine which peaks correspond to which NANF features. We can also use the expressions in [18] to calculate how the time delay between the reference beam and capillary beams changes with the collection angle (Fig. 6(c)). As the collection angle increases, the optical path differences for both the inner and outer NANF capillaries decrease. This is expected, as at more extreme collection angles, in order for the rays to arrive perpendicular to the collection plane, the rays must take a shorter optical path within the fiber jacket.

Optics EXPRESS

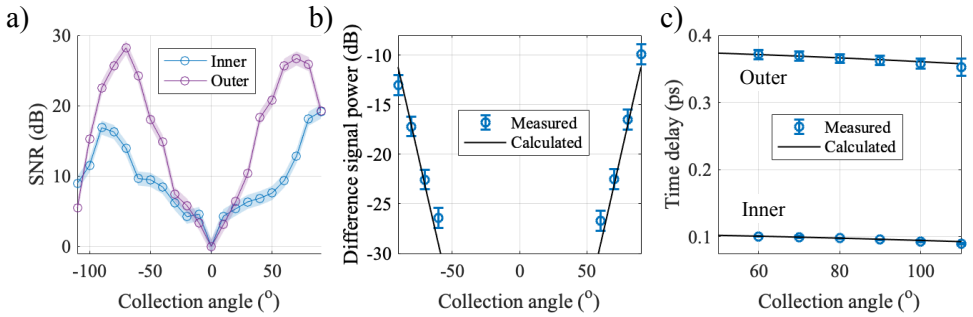

Fig. 6. Effect of collection angle on non-invasive NANF measurement.(a) SNR of inner (blue) and outer (purple) peaks. (b) Power of difference signal relative to mean power of inner and outer peaks. (c) Time delay variation with collection angle for inner and outer capillaries.

3.2. DNANF

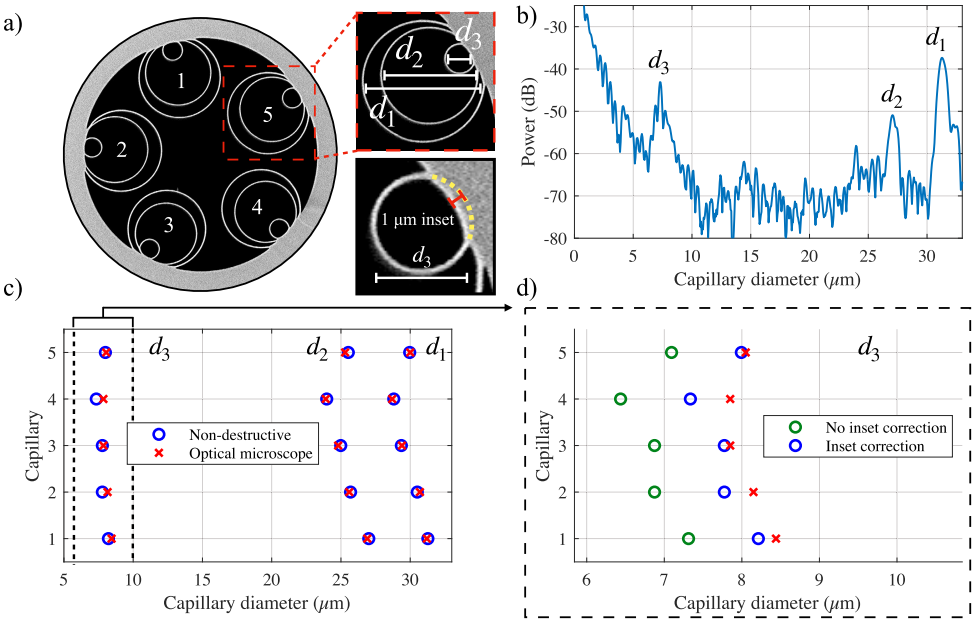

Fig. 7. DNANF results. (a) SEM image of DNANF cross-section. (b) Capillary diameter plot with peaks corresponding to all nested elements. (c) Microscope and non-destructive measurements of DNANF capillaries. (d) Effect of capillary inset on measurements of inner capillary diameter d_3.

Results of a non-destructive measurement of DNANF capillary diameter are shown in Fig. 7. The fiber under test has mean outer, middle and inner capillary diameters of d_1=29.9 µm, d_2=25.4 µm and d_3=8.0 µm (Fig. 7(a)). An example time trace is shown in Fig. 7(b), demonstrating the 3 capillary signals that DNANF is expected to generate. There are 3 peaks for the inner, outer and middle capillaries at 6.8 µm, 25.5 µm and 29.8 µm. We have used a collection angle of 50° to surpress the 3 peaks corresponding to the 3 combinations of pairwise differences. A comparison of microscope and non-destructive measurements of all 5 nested DNANF capillaries is shown

Optics EXPRESS

in Fig. 7. For the middle and outer capillaries there is excellent agreement between the two measurements, with a mean discrepancy of 140 nm (0.6%) for the middle and 90 nm (0.3%) for the outer. For the inner capillary, if scaled using the same method, this mean discrepancy is 14%. This arises due to the effect of the capillary inset, which is only negligible for sufficiently large capillaries and small insets. For small capillaries and large insets - such as the 8.0 μm diameter inner DNANF capillary inset by 1 μm - the inset portion comprises a large proportion of the capillary circumference (23% in this case) and we must correct for this when scaling time domain peaks to capillary diameter (Fig. 7(d)). We must therefore modify the linear scaling presented in Eq. (8) by using the geometrical model to calculate the reduction in optical path that results from a capillary inset of 1 μm into the jacket tube [18]. Doing this reduces the discrepancy to 3%. As this inset value does not vary greatly during the draw process and can be computationally modelled, accurate measurement of these inner capillaries is still possible without needing to cut the fiber and view it under a microscope.

3.3. *Detecting fiber defects*

This technique can also be used to non-destructively detect when neighboring outer capillaries are overinflated and contact each other. If this is the case, while the light is making a round trip of the capillary, a fraction will be coupled into the neighboring tube and will not be picked up by the spectrometer. We can therefore expect to see a reduction in the amplitude of the time domain peaks from contacting capillaries. Figure 8 shows results of measurements of two different NANF samples from the same fiber draw, one with good microstructure (NANF1, Fig. 8(b)) and one with one pair of contacting capillaries (NANF2, Fig. 8(c)). The peak power of the outer capillary signal as the fiber is rotated is plotted in Fig. 8(a). For all five capillaries of NANF1 and capillaries 1-3 of NANF2, the signal peaks at around 0 dB. However, for the contacting capillaries 4 and 5 of NANF2, there is a reduction of around 10 dB in the signal peak, indicating that some light is coupling into the adjacent capillary instead of making a complete round trip. This measurement technique could therefore be used to continuously monitor capillary diameter and determine locations along the fiber where defects occur. Preferably, this technique could be used to prevent capillary contact before it occurs.

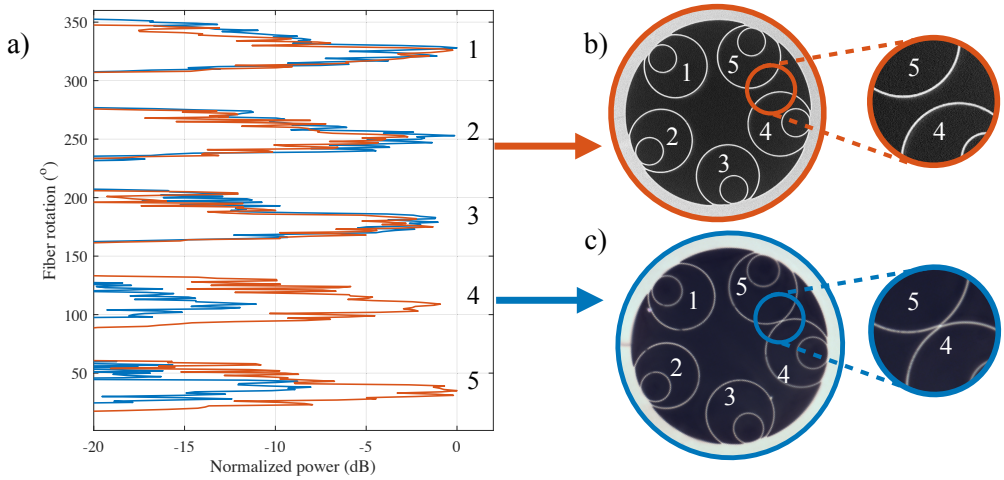

Fig. 8. Detection of contacting capillaries. (a) Outer capillary signal for non-contacting and contacting fiber samples (b) and (c) respectively.

Optics EXPRESS

4. Conclusion

We have demonstrated a technique that can be used to non-destructively measure the microstructure geometry of two promising antiresonant HCF designs, the NANF and the DNANF. This interferometric technique can be well-understood using a simple geometrical optics model and is experimentally straightforward to implement. The scattered spectra exhibit a characteristic interference pattern arising from the time delay between light which traverses the microstructure capillaries and light which reflects off the air-glass interface at the jacket tube. This interference pattern yields peaks in the time domain, corresponding to all the nested capillaries, as well as the various extra peaks at the differences between the nested capillary diameters. The intensity of these peaks is maximized when there is a large spatial overlap between the fields emanating from the nested capillaries. This can lead to the difference signals being of equal or greater magnitude to the capillary signals, resulting in difficulty when trying to determine which peaks correspond to a physical measurement of the capillary diameter. By carefully choosing the angle at which we collect this scattering patter, we show that we can reduce the spatial overlap between the rays, reducing the magnitude of the difference signals and allowing an unambiguous measurement of the capillary diameter. By approximating the capillary itself as a planar waveguide and applying a sensitivity analysis to the other microstructure geometrical parameters, we show here that the time delay is almost entirely dependent on the capillary diameter. We hence apply a linear scaling to the measured time delay peaks and demonstrate that non-destructive measurements of all nested capillary diameters of NANF and DNANF is possible with sub-micron accuracy (<2% in most cases). If the capillaries have a significant inset into the surrounding jacket tube, such as the small inner capillary of DNANF, a straightforward correction for this inset allows accurate measurement. We also show that this technique can be used to determine when adjacent capillaries are overinflated and come into contact with one another, a defect which can drastically reduce fiber performance. When capillary contact occurs, we see a significant reduction in the amplitude of the interference peak, indicating that a portion of the light traversing the capillary has coupled into its neighbor. The speed of taking and analyzing measurements made with this technique make it potentially compatible with inline measurements of NANF and DNANF structure during fabrication.

Funding. RAEng (RF\201819\18\200); ERC (682724).

Disclosures. The authors declare no conflicts of interest.

Data availability. Data underlying the results presented in this paper are not publicly available at this time but may be obtained from the authors upon reasonable request.

References

1. R. F. Cregan, B. J. Mangan, and J. C. Knight, *et al.*, "Single-mode photonic band gap guidance of light in air," Science **285**(5433), 1537–1539 (1999).
2. F. Gérôme, R. Jamier, and J. L. Auguste, *et al.*, "Simplified hollow-core photonic crystal fiber," Opt. Lett. **35**(8), 1157–1159 (2010).
3. F. Poletti, "Nested antiresonant nodeless hollow core fiber," Opt. Express **22**(20), 23807–23828 (2014).
4. G. T. Jasion, H. Sakr, and J. R. Hayes, *et al.*, "0.174 dB/km Hollow Core Double Nested Antiresonant Nodeless Fiber (DNANF)," in *Optical Fiber Communication Conference (OFC) 2022*, paper Th4C.7.
5. W. Belardi, "Design and Properties of Hollow Antiresonant Fibers for the Visible and Near Infrared Spectral Range," J. Lightwave Technol. **33**(21), 4497–4503 (2015).
6. A. F. Kosolapov, G. K. Alagashev, and A. N. Kolyadin, *et al.*, "Hollow-core revolver fibre with a double-capillary reflective cladding," Quantum Electron. **46**(3), 267–270 (2016).
7. V. Michaud-Belleau, E. Numkam Fokoua, and T. D. Bradley, *et al.*, "Backscattering in antiresonant hollow-core fibers: over 40 dB lower than in standard optical fibers," Optica **8**(2), 216–219 (2021).
8. A. Taranta, E. Numkam Fokoua, and S. Abokhamis Mousavi, *et al.*, "Exceptional polarization purity in antiresonant hollow-core optical fibres," Nat. Photonics **14**(8), 504–510 (2020).
9. P. Uebel, M. Günendi, and M. Frosz, *et al.*, "Broadband robustly single-mode hollow-core PCF by resonant filtering of higher-order modes," Opt. Lett. **41**(9), 1961–1964 (2016).
10. L. G. Cohen and P. Glynn, "Dynamic measurement of optical fiber diameter," Rev. Sci. Instrum. **44**(12), 1749–1752 (1973).

Optics EXPRESS

11. D. H. Smithgall, L. S. Watkins, and R. E. Frazee, "High-speed noncontact fiber-diameter measurement using forward light scattering," Appl. Opt. **16**(9), 2395–2402 (1977).
12. S. R. Sandoghchi, G. T. Jasion, and N. V. Wheeler, *et al.*, "X-ray tomography for structural analysis of microstructured and multimaterial optical fibers and preforms," Opt. Express **22**(21), 26181–26192 (2014).
13. A. Stefani, M. H. Frosz, and T. G. Euser, *et al.*, "Real-time Doppler-assisted tomography of microstructured fibers by side-scattering," Opt. Express **22**(21), 25570–25579 (2014).
14. S. Schmidt, T. Tiess, and S. Schröter, *et al.*, "Noninvasive characterization of optical fibers," Opt. Lett. **42**(23), 4946–4949 (2017).
15. M. H. Frosz, R. Pennetta, and M. T. Enders, *et al.*, "Non-invasive real-time characterization of hollow-core photonic crystal fibers using whispering gallery mode spectroscopy," Opt. Express **27**(21), 30842–30851 (2019).
16. L. Budd, A. Taranta, and E. N. Fokoua, *et al.*, "Non-Invasive Measurement of Hollow-Core Antiresonant Fiber Structure," in *2021 IEEE Photonics Conference (IPC)* (IEEE, 2021), pp. 1–2.
17. L. Budd, A. Taranta, and E. N. Fokoua, *et al.*, "Non-Destructive Structural Characterisation of Double Nested Antiresonant Nodeless Fiber," in *Optica Advanced Photonics Congress 2022, Technical Digest Series* (Optica Publishing Group, 2022), paper SoTh3G.1.
18. Y. Xiong, S. She, and Y. Sun, *et al.*, "Four-ray interference model for complete characterization of tubular anti-resonant hollow-core fibers," Opt. Express **30**(26), 48061–48074 (2022).
19. E. A. J. Marcatili, "Bends in Optical Dielectric Guides," Bell Syst. Tech. J. **48**(7), 2103–2132 (1969).